The DOE Award Number:	**DE-FG07-07ID14770**
Name of recipient:	Rensselaer Polytechnic Institute
Date of Final Report:	Due Jan 28, 2011
Report period:	May 1, 2007 - Oct 30, 2010
Project title:	**Bioassay Phantoms Using Medical Images and Computer Aided Manufacturing**

Author: Dr. X. George Xu, Principal Investigator
Professor of Nuclear Engineering and Biomedical Engineering
Rensselaer Polytechnic Institute
Room 1-11, Tibbits Ave.
Troy, New York 12180
Tel: 518-276-4014
Fax: 518-276-4832
E-mail: xug2@rpi.edu

A radiation bioassay program relies on a set of standard human phantoms to calibrate and assess radioactivity levels inside a human body for radiation protection and nuclear medicine imaging purposes. However, the methodologies in the development and application of anthropomorphic phantoms, both physical and computational, had mostly remained the same for the past 40 years. We herein propose a 3-year research project to develop medical image-based physical and computational phantoms specifically for radiation bioassay applications involving internally deposited radionuclides. The broad, long-term objective of this research was to set the foundation for a systematic paradigm shift away from the anatomically crude phantoms in existence today to realistic and ultimately individual-specific bioassay methodologies. This long-term objective is expected to impact all areas of radiation bioassay involving nuclear power plants, U.S. DOE laboratories, and nuclear medicine clinics.

In preliminary studies performed prior to 2005 at Rensselaer and elsewhere had shown that organ dose data obtained using the existing stylized phantoms differed remarkably from human models defined by medical CT, MR and the Visible Human images. Therefore, it was believed when we submitted the proposal to DOE that a new bioassay phantom paradigm based on 3-dimensional (3D) anatomical images and integrated with modern Monte Carlo simulation tools, could significantly improve the quality of in-vivo radiation bioassay measurements. Although our previous studies had made crucial breakthroughs, relatively little experience existed on how to efficiently fabricate useable physical phantoms from anatomical images. Computer aided design (CAD) and manufacturing (CAM) have been available for industrial applications, but were not explored for human phantom fabrication. For almost 30 years, the radiation dosimetry community had relied on anatomically crude bioassay phantoms to calibrate whole-body counters.

This 3-year project was proposed and funded to achieve the following Specific Aims:

1. To study methods of modeling human body from segmented and labeled 3D medical images
2. To develop a "3D printing" rapid prototyping technique for fabricating physical phantoms from 3D medical image-based human models and for mixing radioactive materials into selected organs
3. To develop and test a method of "virtual calibration" for bioassay systems using the image-based, size-adjustable computational phantom and specialized Monte Carlo detector models
4. To demonstrate the feasibility of applying these advanced tools for radiation protection and nuclear medicine bioassay
5. To establish and maintain a national center of bioassay phantoms for the radiation dosimetry community and an internet-based dissemination channel that will allow for efficient data-sharing, intercomparisons and standardization.

In this final report of the project, we summarize major findings:

Task 1.

In this task, we developed and investigated methods to define and visualize 3D human organs using the whole-body Visible Human images. The Visible Man data include three sets of digital images obtained separately from CT, MRI, and color photographs of a cryosectioned body of a 39-y-old male. The color photos we used have a pixel size of 0.33-mm x 0.33-mm with a slice thickness of 1-mm, making this set of images the finest whole-body data available in the U.S. Smaller voxel sizes would likely to represent the geometry more accurately. In addition, the color information in the images would allow for easier identification of radiosensitive structures. These unique features facilitated the image segmentation process that was critical in constructing a tomographic human model. The term "segmentation" means the process of identifying the tissues and organs of interested and then assigning

special ID numbers to each of the organs. Fig. 1 illustrates the process of segmenting the original image. For radiation protection applications, about 80 critical tissues/organs are of interest.

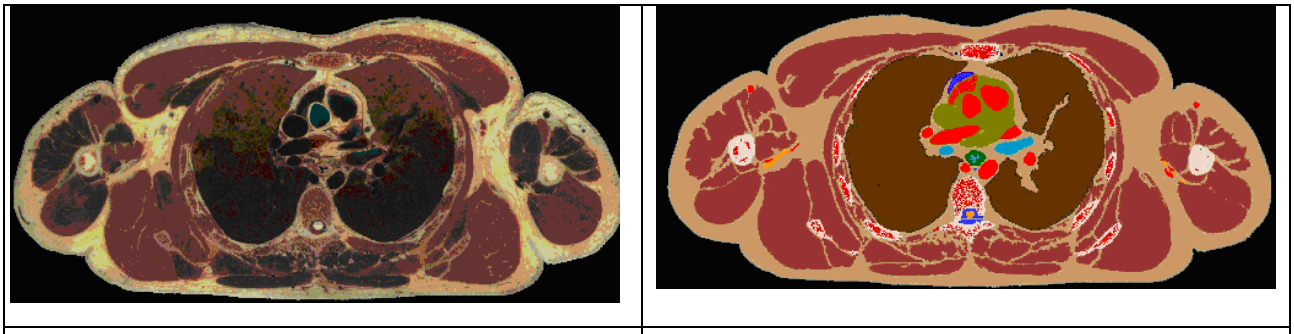

(a) (b)

Fig. 1. Segmentation process. (a) Original transversal color image at the chest level. (b) The same slice after segmentation and classification containing only important organs and tissues.

In order to create a physical phantom of an organ such as the lung, the medical images have to be processed to define the 3D boundary of the organ. Little experience existed on how to use medical images to fabricate a physical phantom. Through this project, we developed considerable expertise in segmenting Visible Man images and to translate the voxelized data into 3D polygon mesh models using a code written in tcl/tk. The tcl program generates different organs as Visualization Toolkit (VTK) files. A VTK file is a 3D polygon mesh file of an organ which was further converted into a stereolithography (STL) file. The STL files were corrected and scaled to the actual size of organs. Once the organs were scaled and they were hollowed out to avoid distortion during the 3D printing (to be described below) and to save the printing material. Once the files were completed, they were sent to a 3D printer for rapid prototyping. Using the Rhinoceros 4.0 software (Robert McNeel & Associates, Seattle, WA), a polygon surface mesh model of the VIP-Man's right lung was edited and converted to stereolithography (STL) format ready for rapid prototyping as shown in Fig. 2). This surface mesh model, is based on images from the Visible Human Dataset supplied by the US National Library of Medicine and has a volume of 1771 cm^3. In preparation for the prototyping, the lung polygon mesh model was "hollowed out" using the Rhinoceros 4.0 software to reduce construction costs. The prototyping cost associated with the Z-Corp machine depends on the volume the part being fabricated (≈\$3/$inch^3$). The "hollowed out" lung shell model had a wall thickness of 0.5 cm and a total volume of 28 cubic inches. Yet, the user will not benefit from the reduced construction cost of the "hollow" lung model unless the unused plaster powder, the material used to fabricate the part, can actually be removed from the prototype. To this end, the lung shell model was split into two halves which can be prototyped separately and then attached together with an adhesive.

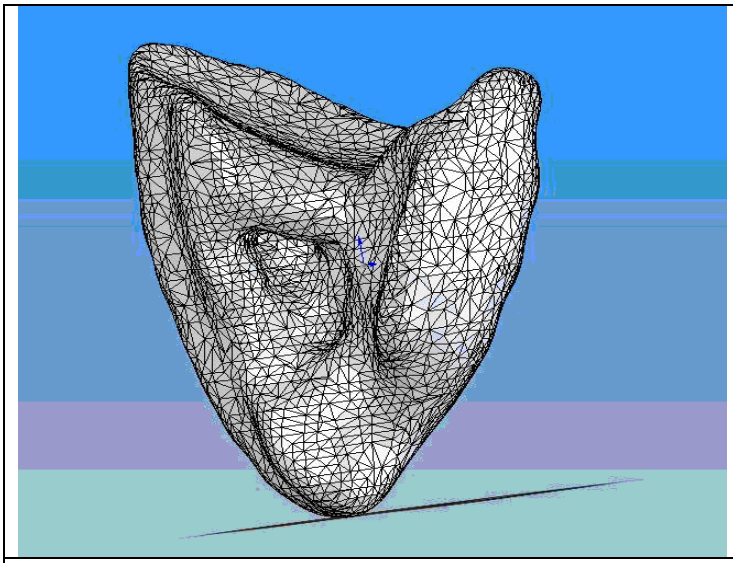

Fig 2: (a) A 3D display of the lung in the STL format.

Task 2.
A lung phantom designed for bioassay applications should have the following characteristics: 1) The geometry of the phantom should be similar to a real human lung; 2) The phantom lung should be made of a material which mimics, as closely as possible, the radiation attenuation properties of real human lung over a specified range of gamma-ray energies. This means the phantom lung should have a density of roughly 0.26 g/cm^3 and an effective atomic number of about 7.49. ; 3) A known amount of radioactivity should be spread uniformly throughout the model.

The fabrication of a plaster model of the right lung of the VIP Man virtual phantom was done using a Z-Corp Z402 3D Printer available in Rensselaer's Advanced Manufacturing Laboratory. To reduce prototyping costs, the prototyped lung was "hollowed out" and split into two halves which were later attached using wood glue. The resulting plaster model was used as the basis for the creation of a rubber mold from which tissue equivalent copies can be cast out of Foamex XRS-272 polyurethane foam (Foamex Polyurethane Products Co. Inc., Santa Fe Springs, CA).

The prototyping used a Room Temperature Vulcanizing (RTV) silicone rubber known as OOMOO 30 (Smooth-On, Easton, PA). OOMOO 30 is a low viscosity, tin-cured silicone rubber which is unique in that it does not require vacuum degassing. Silicone rubber is an ideal material for making a mold because of its flexibility, its ability to reproduce the exact detail, its long mold life which allows for multiple reproductions, and its good mold release properties. OOMOO 30 comes in two parts, denoted as Part A and Part B respectively. To make the silicone rubber, Parts A and B were mixed in equal parts by volume. The OOMOO 30 has a pot life of 30 minutes and is fully cured after 6 hours. The resulting silicone rubber has a Shore hardness of 30A.

To create the two-part silicone rubber mold, a wood mold box large enough to contain hold the plaster model was used to contain the silicone rubber. The box consists of two halves (a top and a bottom) which sit on top of each other and are secured with six metal latches, two on each side (Fig. 3). A small hole was cut out of the top and bottom of the mold box using a spade drill bit (Fig. 4). These holes were used for pouring the silicone rubber mold. Small pieces of wood were then glued into the box and secured with screws so as to fill up some of the volume, thus minimizing the amount of expensive silicone rubber needed for the mold (Fig. 5).

Fig. 3. Empty mold box

Fig. 4 A pour hole is cut in the top and bottom of the box.

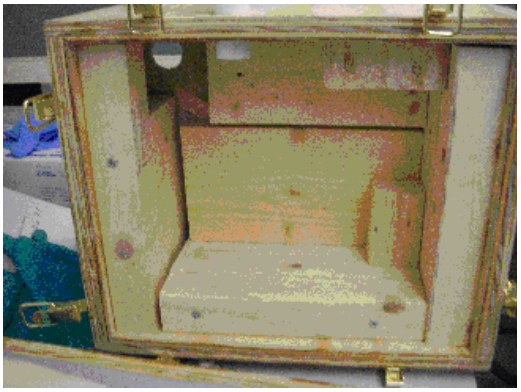

Fig. 5. Wood is glued in the box to fill up the excess volume.

Next, the bottom half of the box was filled with rice and the model is lowered into the box (Fig. 6). The rice is convenient because it allows for easy positioning of the model in the box. The model is should be at least 2 cm from all sides of the wood box and the dividing line between two halves of the molds should be chosen very carefully to ensure that there are no severe undercuts which may ultimately prevent the model from releasing from the mold. The remainder of the bottom half of the mold box was then filled with a layer of clay to define the dividing line between the two halves of the rubber mold. Mold keys were created by forming indentations in the clay (Fig. 7). It is important to use clay which does not contain sulfur as this will inhibit the silicone from curing. The portions of the plaster model protruding through the clay were then covered with petroleum jelly which acted as a release agent. The top half and bottom halves of the box were then secured together and enough silicone rubber was poured through the hole in the top of the box to make the first half of the mold (Figs. 8-10). It is important to make sure that the silicone rubber is mixed very well and that it is poured uniformly to help minimize entrapped air. The rubber will seek its own level and will cover the model.

Fig. 6. The mold is buried in rice in the box.

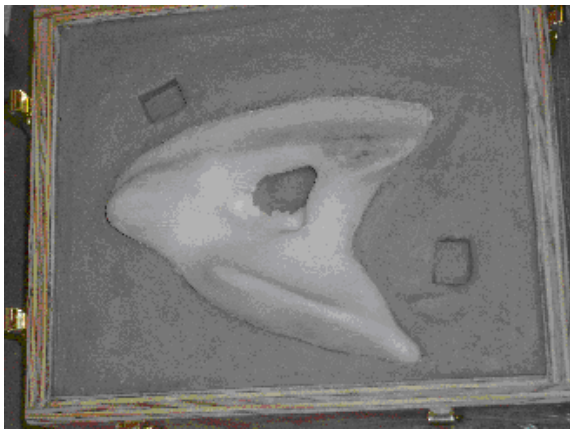

Fig. 7. A layer of clay is used to define the parting line between the two halves of the mold. Mold keys are made by making indentations in the clay.

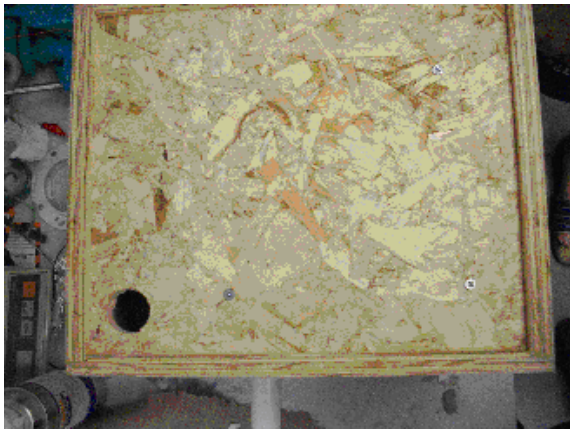

Fig. 8. The top of the box is secured to the bottom in preparation for pouring the first half of the mold.

Fig. 9. A cup acts was used as a makeshift funnel to get the silicone into the box.

Fig. 10. The box is filled to the top with purple liquid silicone rubber. The rubber cures in 6 hours.

Each half of the two-piece mold is poured separately. Once the rubber in the first half of the mold has cured, the box can be opened so that the clay and rice can be removed. This should be done very carefully so as not to destroy the fragile plaster model. Unfortunately, in our first attempt at opening the box, our plaster model broke into many pieces (Fig. 11). Using clay, however, we were able to sculpt the model back together (Figs. 12-15). Ways of strengthening the plaster models to prevent breakage will be examined in the future.

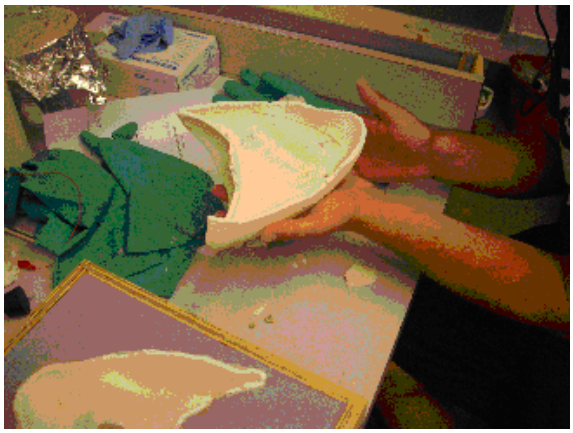

Fig. 11. Upon opening the box to reveal the first half of the rubber mold, the fragile plaster model shattered into many pieces.

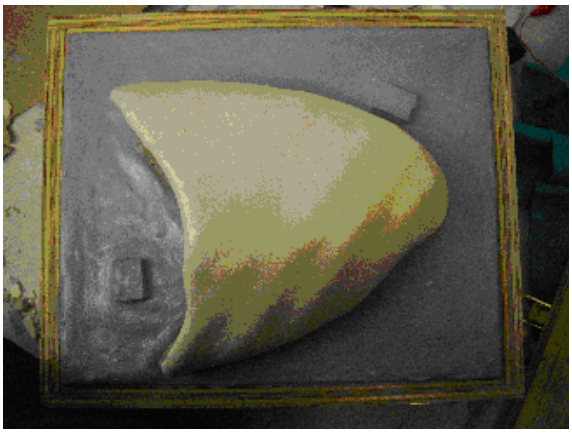

Fig. 12. A top view of the fixed lung model. The model was fixed by carefully piecing it together and sculpting it with clay.

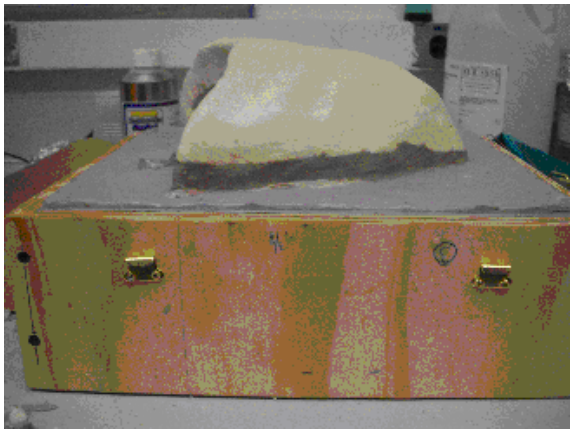

Fig. 13. View of the fixed lung model from the left.

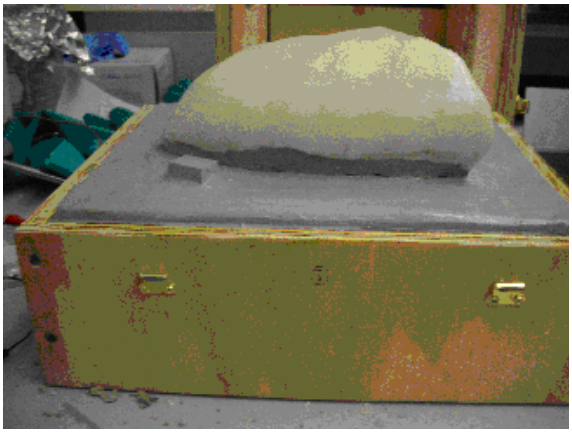

Fig. 14. View of the fixed lung from the right.

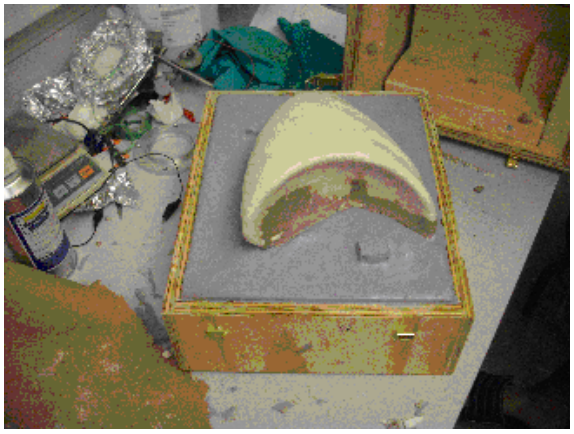

Fig. 15. Side view of the fixed lung model.

The first half of the silicone mold was then cleaned in preparation for the pouring of the second half of the mold. The plaster model and the visible silicone were covered with petroleum jelly release agent. To create a pour hole for the mold, a 1'' diameter hole was cut through the side of the bottom half of the mold box. The top and bottom halves of the box were secured together, this time with the bottom of the box face up. A small piece of 1'' diameter PVC piping was then run through the hole in the side of the box. The PVC piping was filled with clay to prevent silicone from leaking out. Finally, enough silicone was poured through the hole in the bottom of the box (now face up) to create the second half of the mold. Once the second half of the silicone mold has fully cured, the box was placed on its side and the PVC piping was removed. The small cylindrical void in the silicone left by the PVC piping is then covered with petroleum jelly release agent and then filled with silicone rubber to create a custom, removable rubber stopper (Fig. 16-18). The two halves of the box were carefully pried apart revealing the final mold of the lung model (Fig. 17). Unfortunately, the fragile plaster lung model could not be demolded from the silicone rubber intact. The plaster model was ultimately destroyed during the demolding process.

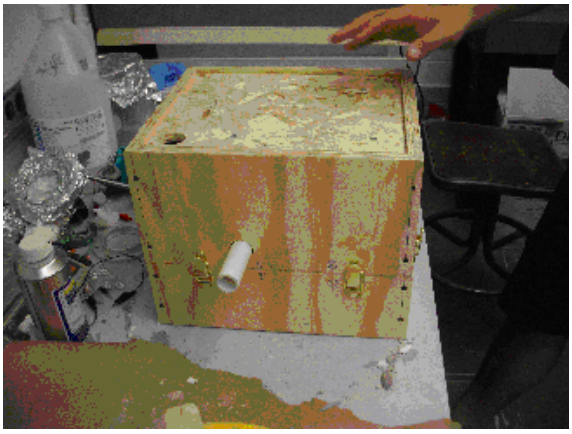

Fig. 16. PVC piping is used to create a rubber stopper which can be inserted in the side of the box.

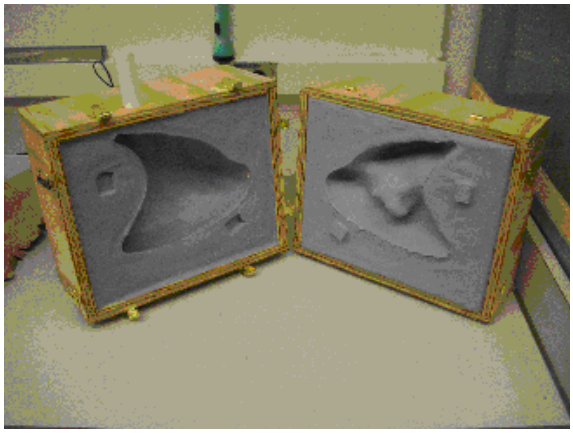

Fig. 17. The final lung mold.

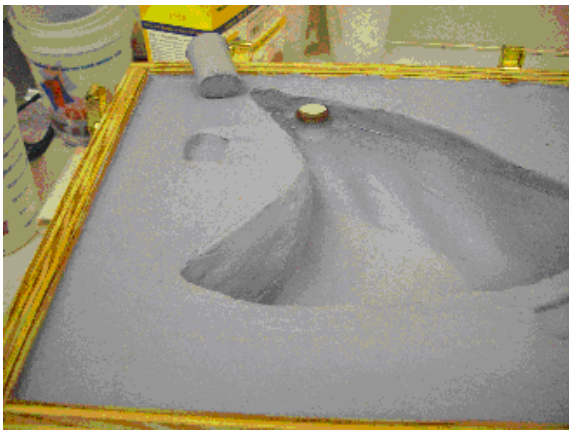

Fig. 18. The rubber stopper and pour hole.

Fig. 19. The pour hole as viewed from outside the mold box.

The lung mold has been used in an attempt to create tissue equivalent copies using the Foamex XRS-272 flexible polyurethane foam. The volume of the lung mold is estimated to be roughly 1917 cm^3. Thus, if we would like a lung with a density of 0.26 g/cm^3, a total of roughly 438 grams of polyurethane foam material must be added to the mold. Initial attempts at producing lungs of proper density appear promising; however, there are still some challenges to overcome. During the molding process, the necessary 438 grams of polyurethane foam exerts such great force on the two halves of the mold are push apart, despite the fact that they are secured with six latches. This produces an excessive amount of mold flashing that inhibits the creation of phantom lungs of the desired density. On recommendation from experienced scientist, we have added extra support to our mold box by using two aluminum plates connected by threaded metal rod (Figs. 20-23). Now that this support has been built, new phantom lung fabrication trials are currently underway with the modified box. Small air vents may eventually be added to allow the gas within the mold to escape.

Fig. 24 shows a few polyurethane foam models which were cast using the lung mold. The highest density foam lung created so far is 0.195 g/cm^3.Once a polyurethane foam lung with a density of 0.26 g/cm^3 has been fabricated, calcium carbonate will be added to the foaming material to raise the electron density. It may be of future interest to investigate how to measure the elemental content of the polyurethane foam. The manufacturer of the Foamex XRS-272 considers this information proprietary. This information will be needed in order to calculate how much calcium carbonate should be added to the foam to obtain the desired radiation attenuation characteristics.

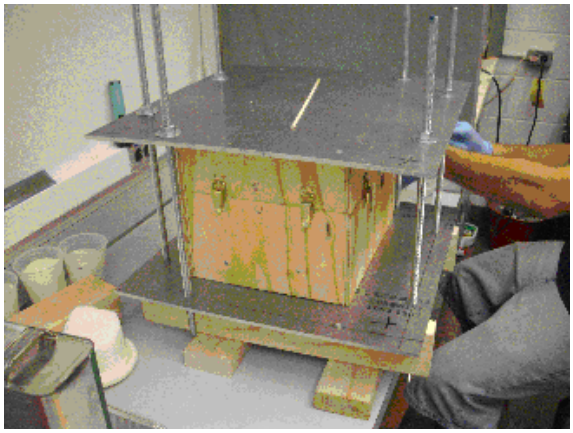

Fig. 20. View of the mold box supported by aluminum plates.

Fig. 21. An isometric view of a CAD model of the mold box

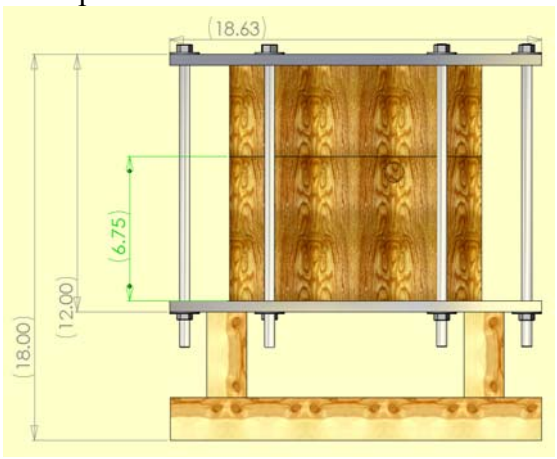

Fig. 22. Front view of the CAD model of mold box with dimensions labeled in inches.

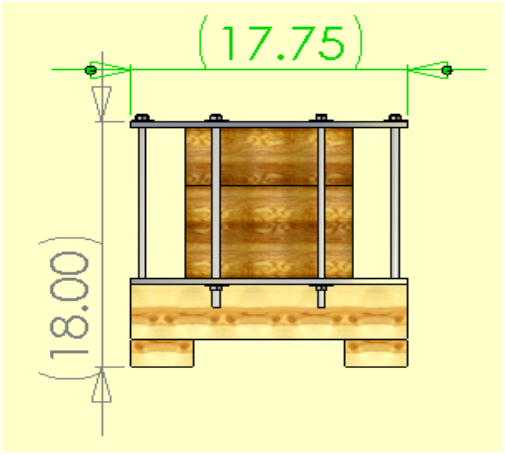

Fig. 23 Side view of the CAD model of the mold box with dimensions labeled in inches.

Fig. 24. A few polyurethane foam models which were cast using the lung mold. The highest density foam lung created so far is 0.195 g/cm^3.

Task 3.

We have collected many virtual phantoms to create a library for research. This includes the VIP-Man, NORMAN, BOMAB, JAEA and a Chinese phantom called CHMAN. In addition, we processed CT images for the Lawrence Livermore National Laboratory (LLNL) phantom. Computed tomography images of a second generation LLNL torso phantom were solicited. DICOM formatted images of the physical phantom were segmented into four materials (bone, lung, soft tissue, and air) using the software packages 3D-DOCTOR and MATLAB. Other software, which was developed in-house at RPI, was used to convert these segmented images into a voxel-based model of the LLNL torso suitable

for implementation in Monte Carlo radiation transport calculations. The material definitions for the virtual phantom were specified using relevant data from the manufacturer found in the literature.

We have used the Monte Carlo N-Particle Transport Code to compare the counting efficiencies of virtual models of physical phantoms (BOMAB, LLNL, JAERI, and RANDO®) and tomographic models based on images of real individuals (VIP-Man, NORMAN, and CNMAN) for typical whole-body. The results reveal that a phantom's counting efficiency is strongly dependent on the shape and size of a phantom. Contrary to what was expected, it was found that only small differences in efficiency were observed when the density and material composition of all internal organs and tissues of the tomographic phantoms were changed to water. The results of this study indicate that BOMAB phantoms with appropriately adjusted size and shape can be sufficient for whole-body counting calibrations when the internal contamination is homogeneous.

Task 4.

To demonstrate the feasibility of applying these advanced modeling tools to internal radiation dosimetry for nuclear workers working in DOE facilities (i.e., bioassay), we have performed systematical simulations of the HPGe detector for a library of voxel phantoms discussed under Task 3. This task allows us to establish a database for bioassay counting efficiency for individuals with various body sizes. To optimize the detector model, several parameters were first investigated including the use of Mylar layer, the use of aluminum layer, the thickness of the magnesium layer, the thickness of the inner and outer dead layers and the radius of the torus. Comparison between experimental results and Monte Carlo computation for 5ml Ga-67 Ampoule showed that one of the major factors that influence the data consistency is the torus used to describes the round front corners of the crystal. Contrary to our expectations, when the torus is not used, Monte Carlo computation for the Ampoule phantom seems to be in better agreement with the experiment. Besides, at low energy region (93.3keV) the difference between Monte Carlo computation and experiment can be as large as ~10%. Five phantoms have been used to virtually calibrate the detector. They are 5ml Ampoule phantom, Bottle Manikin ABsorption (BOMAB) phantom, RPI Adult Male phantom in a sitting posture, the Lawrence Livermore National Laboratory (LLNL) realistic torso phantom, and the Japanese Atomic Energy Research Institute (JAERI) realistic torso phantom. The head of BOMAB was also used separately because its experimental data is available to compare with Monte Carlo computation. Ampoule and BOMAB are stylized phantoms, composed of simple geometries such as ellipsoid and cylinder. The liquid filled inside these geometries contains radionuclides spiked with known amount of activity. RPI Adult Male, LLNL and JAERI are voxel phantoms. For RPI Adult Male, the source is assumed to be uniformly distributed all over the body. For LLNL and JAERI, only the lung is assumed to be contaminated with radionuclides.

For each phantom there are two variables in our Monte Carlo computation. One is the distance between the detector and the phantom; the other is the energy of the gamma radiation emitted by the source. We put the phantoms in the centerline of the detector model and run the computation under varying distances. Ampoule and BOMAB-Head are placed100, 110, 120, 130 cm away from the detector. BOMAB-Whole Body and RPI Adult Male are placed 300 cm away, and LLNL and JAERI 200 cm away. Note that the difference in the distance setting results from the requirement that the phantom be entirely covered by the solid angle of the germanium crystal of the detector. As to the energy, we selected 26 different points ranging from 93.3keV to 1333.5keV (listed below). The interval between two energies is around 50 keV, and each energy is related to a specific radionuclide. For instance, the 93.3 keV gamma radiation is emitted by Gallium-67, and the 1333.5 keV emitted by Cobalt-60. Sufficient particle histories were simulated to ensure that the Monte Carlo statistical uncertainty was less than 5%.

Task 5.
One of the aims of the project was to gather and disseminate the information to the bioassay user community. We have built a website where information related phantoms. So far, we have registered a domain name and established the framework for a Consortium of Computational Human Phantoms (www.virtualphantoms.org). This is the beginning of an effort to establish this website into a portal for educational and research activities including standardization and intercomparison. During the projects, a number of peer-reviewed papers and conference presentations have been published citing this and other related grant support. A list of these publications from this project is given below.

Publications from this project

1. Zhang B, Mille M, and Xu XG. An analysis of dependency of counting efficiency on worker anatomy for in-vivo measurements: whole-body counting. Phys. Med. Biol. 53: 3463-3475. 2008.
2. Mille M., Zhang BQ., Xu, XG. An Analysis of the Dependency of Lung Counting efficiency on Specific Anatomy in Selected Physical and Tomographic Phantoms. HPS Summer Meeting 2008.
3. Mille M., Xu, XG. Fabrication of Human Organs for Realistic Calibration Phantoms by Rapid Prototyping. HPS Summer Meeting, 2008.
4. Zhang B, Mille M, Xu XG. Monte-Carlo "Virtual" Calibration of Counting Efficiency for Assessing Patient Internal Radioactivity Burden Using Organ-adjustable RPI Adult Male Phantom. AAPM Summer Meeting, 2008.
5. Zhang BQ, Mille M, Xu XG. An Analysis of the Dependency of Whole-body Counting Efficiency on Specific Anatomy in Selected BOMAB and Tomographic Phantoms. HPS Summer Meeting, 2008.
6. Hegenbart L, Na YH, Zhang* JY, Urban M, Xu XG. A Monte Carlo study of lung counting efficiency for female workers of different breast sizes using deformable phantoms. Phys. Med. Biol. 53:5527-5538, 2008.
7. Mille M, Hegenbart L, Na Y, Zhang J, Xu XG. Deformable computational breast phantoms for Monte Carlo based calibrations of detector systems used for assessing internal radioactivity burden in the lungs. AAPM Summer Meeting, 2009.
8. Hegenbart L, Mille M, Na YH, Zhang J, Ding A, Urban M, Xu XG. Investigation Of The Effect Of Female Breast Size on Lung Counting Efficiency Using Virtual Deformable Phantoms. HPS Summer Meeting, 2009.
9. Mille M, Zhang B, Xu XG. Specific Absorbed Fractions for Photon Emitters Calculated for the RPI-Adult Male and Female Phantoms. HPS Summer Meeting, 2009.
10. Mille M, Hegenbart L, Na Y, Zhang J, Xu XG. Deformable computational breast phantoms for Monte Carlo based calibrations of detector systems used for assessing internal radioactivity burden in the lungs. Med. Phys. 36(6): 2620-2621, 2009.
11. Liu T, Mille M, Caracappa PF, Xu XG, Nour S, Inn K. A Software Solution to Bioassay Detector Calibration Using A Library of Virtual Phantoms. Health Phys. 99(1): S78, 2010.
12. Han B, Na YH, Caracappa PF, Xu XG. Monte Carlo Modeling of a Sitting Phantom for Improved Environmental Dose Assessment. Health Phys. 99(1): S59, 2010.